Omni-Plus-Seven (O 7 +): An Omnidirectional Aerial Prototype with Minimal Uni-directional Thrusters

Mahmoud Hamandi, Kapil Sawant, Marco Tognon, Antonio Franchi

Omni-Plus-Seven (O^7_+): An Omnidirectional Aerial Prototype with Minimal Uni-directional Thrusters

Mahmoud Hamandi[1], Kapil Sawant[1], Marco Tognon[1], Antonio Franchi[2,1]

***Abstract*— The aim of this paper is to present the design of a novel omnidirectional Unmanned Aerial Vehicle (UAV) with seven uni-directional thrusters, O^7_+. The paper formally defines the O_+ design for a generic number of propellers and presents its necessary conditions; then it illustrates a method to optimize the placement and orientation of the platform's propellers to achieve a balanced O_+ design. The paper then details the choice of the parameters of the O^7_+ UAV, and highlights the required mechanical and electrical components. The resultant platform is tested in simulation, before being implemented as a prototype. The prototype is firstly static-bench tested to match its nominal and physical models, followed by hovering tests in multiple orientations. The presented prototype shows the ability to fly horizontally, upside down and at a tilted angle.**

I. INTRODUCTION

Unamanned Aerial Vehicles (UAVs) have been widely studied in the literature, with many applications that attempted to push the ability of these vehicles to their limits, such as aerial physical interaction [1], [2], surveying, photography, hobby racing, etc.

In its generic form, a UAV hovering (or flying) in the three-dimensional world is a rigid body able to apply forces and moments in (at most) a six-dimensional space. The applied forces and moments usually have the task to counteract external forces such as gravity, wind, etc, in addition to internal and external gyroscopic effects. The applied control wrench is generally allocated with a group of motors placed around the CoM, with fixed or actuated orientations, and whose placement and aerodynamic properties define the shape of the platform's wrench space.

The most common UAV example in the literature is the quadrotor [3], [4], which can apply uni-directional forces and three-dimensional moments. Given its wrench space, such a vehicle modifies its orientation to be able to move in the three-dimensional world.

To decouple the platform's forces from its orientation, multiple designs in the literature presented platform's that exploit the full six-dimensional wrench space. [5] and [6] use tilted uni-directional thrusters to apply forces in $\mathbb{R}^3$ independently from the applied moment. However, the set of feasible forces applied by these platforms does not span the entire $\mathbb{R}^3$. Thus, the feasible tilting angle from their horizontal orientation is limited.

Conversly, other works actively tilt the propellers to achieve omnidirectional flight: [7] synchronizes the tilt angle of the propellers of a hexarotor, [8] actively tilts the angles of a quadrotor independently about their radial axes, and [9] actively tilts the propellers of a trirotor, while adding a fixed central propeller to carry the weight of the vehicle. While popular in the literature, actuated propellers add weight to the platform due to the extra actuators; in addition, propeller tilting is achieved via servo motors, which cannot guarantee instantaneous force excertion because of the time required to re-orient the propellers.

On the other hand, [10]–[12] achieve omnidirectional flight with 6 or 8 bidirectional thrusters. While their solutions are very interesting, as illustrated in [13], bidirectional thrusters exhibit a singularity near the zero thrust region. Moreover, commercial hardware solutions for bidirectional thrust are not satisfactory, where commercial ESCs allowing the control of bidirectional propellers are scarce. Additionally, bidirectional propellers provide less thrust than their uni-directional equivalent.

In our previous work [14], we investigated the required properties and conditions to achieve omnidirectional flight with fixed uni-directional thrusters. We proved the number of propellers $n \geq 7$ to be a necessary condition. Furthermore, we presented an optimization method to find propeller tilts for any generic number of propellers $n \geq 7$, that can guarantee the omnidirectional property of the platform, while enforcing equal sharing of the desired forces over all propellers.

In this work we aim to design, manufacture and test an omnidirectional platform with the minimal number ($n = 7$) of uni-directional thrusters. Our design will rely on the optimization proposed in [14]. To the knowledge of the authors, this is the first manuscript in the literature showing such a working prototype with above mentioned properties; the manufactured platform is shown in Fig. 1.

The rest of this paper is organized as follows. In section II we model a generic UAV platform. In sections III and IV we define the properties that guarantee the omnidirectionality of a platform with uni-directional thrusters, and define the optimization problem with an emphasis on the assumptions we made for our prototype. Section V presents the controller used to fly the platform, wile section VI presents the final prototype. Sections VII-IX show the numerical and real experiments that test the feasibility of the platform. Finally,

[1]LAAS-CNRS, Université de Toulouse, CNRS, Toulouse, France, mahmoud.hamandi@laas.fr, kapil.sawant@laas.fr, marco.tognon@laas.fr, antonio.franchi@laas.fr,

[2]Robotics and Mechatronics lab, Faculty of Electrical Engineering, Mathematics & Computer Science, University of Twente, Enschede, The Netherlands a.franchi@utwente.nl

This work was partially funded by the European Union's Horizon 2020 research and innovation programme under grant agreement ID: 871479 AERIAL-CORE

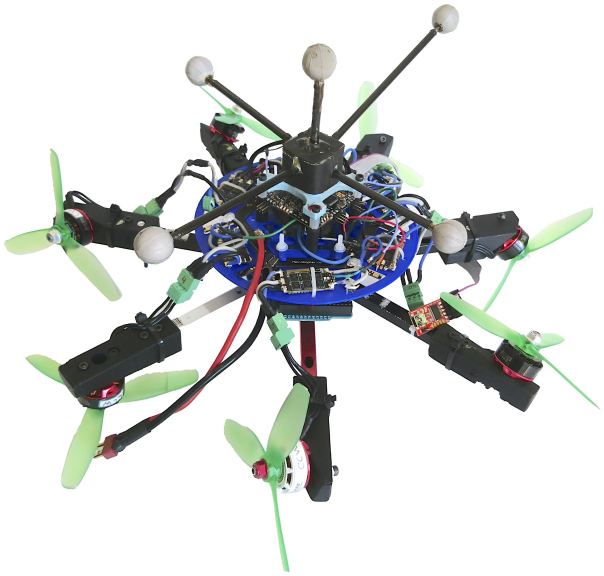

Fig. 1: The built prototype showing the motor assembly, the electronics assembly and the motion capture tracking markers.

section X concludes the paper.

II. Modeling

Let us define a world frame $\mathcal{F}_W$ with origin O_W following the East-North-Up (ENU) convention with axes $\{\boldsymbol{x}_W, \boldsymbol{y}_W, \boldsymbol{z}_W\}$. Let us define a body frame $\mathcal{F}_R$ with center O_R fixed to the geometric center of the robot (assumed to coincide with the robot's center of mass, CoM), with axes $\{\boldsymbol{x}_R, \boldsymbol{y}_R, \boldsymbol{z}_R\}$. We refer to $\boldsymbol{p}_R \in \mathbb{R}^3$ as the position of O_R in $\mathcal{F}_W$ and to $\boldsymbol{R}_R \in SO(3)$ [1] as the orientation of $\mathcal{F}_R$ with respect to (w.r.t.) $\mathcal{F}_W$– we refer to ϕ, θ, ψ as the corresponding roll, pitch and yaw of the rotation $\boldsymbol{R}_R$. We refer to $\boldsymbol{v}_R \in \mathbb{R}^3$ as the translational velocity of O_R in $\mathcal{F}_W$, and to $\boldsymbol{\omega}_R \in \mathbb{R}^3$ as the angular velocity of $\mathcal{F}_R$ w.r.t. $\mathcal{F}_W$, expressed into $\mathcal{F}_R$.

Let $m_R \in \mathbb{R}_{>0}$ and $\boldsymbol{J}_R \in \mathbb{R}^{3\times3}_{>0}$ define the mass and the positive definite inertia matrix of the robot w.r.t. $\mathcal{F}_R$. Then, following the Newton-Euler formalism, we can write the robot equations of motion as $\dot{\boldsymbol{p}}_R = \boldsymbol{v}_R$, $\dot{\boldsymbol{R}}_R = \boldsymbol{R}_R \Omega_R$, and

$$\begin{bmatrix} m_R \dot{\boldsymbol{v}}_R \\ \boldsymbol{J}_R \dot{\boldsymbol{\omega}}_R \end{bmatrix} = -\begin{bmatrix} g\, m_R \boldsymbol{e}_3 \\ \boldsymbol{\omega}_R \times \boldsymbol{J}_R \boldsymbol{\omega}_R \end{bmatrix} + \boldsymbol{G}\,\boldsymbol{w}, \tag{1}$$

where $\Omega_R = \boldsymbol{S}(\boldsymbol{\omega}_R)$ is the skew symmetric matrix relative to $\boldsymbol{\omega}_R$, $\boldsymbol{e}_3 = [0\ 0\ 1]^\top$, g is the gravitational constant, and $\boldsymbol{w} \in \mathbb{R}^{6\times1}$ is the total wrench applied on O_R w.r.t. $\mathcal{F}_R$ such that (s.t.) $\boldsymbol{w} = [\boldsymbol{f}^\top\ \boldsymbol{m}^\top]^\top$, where $\boldsymbol{f} \in \mathbb{R}^3$ and $\boldsymbol{m} \in \mathbb{R}^3$ are the corresponding force and moment components of $\boldsymbol{w}$. Finally, $\boldsymbol{G}$ is the 6-by-6 matrix of the form

$$\boldsymbol{G} = \begin{bmatrix} \boldsymbol{R}_R & \boldsymbol{0}_3 \\ \boldsymbol{0}_3 & \boldsymbol{I}_3 \end{bmatrix} \tag{2}$$

We denote by n as the number of propellers, and by $\boldsymbol{F} \in \mathbb{R}^{6\times n}$ as the full allocation matrix, $\boldsymbol{F}_1 \in \mathbb{R}^{3\times n}$ and $\boldsymbol{F}_2 \in \mathbb{R}^{3\times n}$ as the force and moment allocation matrix, s.t.

$$\boldsymbol{w} = [\boldsymbol{F}_1^\top\ \boldsymbol{F}_2^\top]^\top [u_1 \quad \dots \quad u_n]^\top = \boldsymbol{F}\boldsymbol{u}, \tag{3}$$

where u_i is the control thrust of the corresponding $i-$th propeller, and $\boldsymbol{u} \in \mathbb{R}^{n\times1}$ their concatenation. It is noted that in this formalism it was assumed that the propellers are the only source of wrench being applied on the robot, and that any other sources are neglected as secondary disturbance. $\boldsymbol{F}_1$ and $\boldsymbol{F}_2$ can be written as follows:

$$\boldsymbol{F}_1 = [\boldsymbol{v}_1 \quad \dots \quad \boldsymbol{v}_n], \tag{4}$$

$$\boldsymbol{F}_2 = [\boldsymbol{d}_1 \times \boldsymbol{v}_1 \quad \dots \quad \boldsymbol{d}_n \times \boldsymbol{v}_n] + [c_1 k \boldsymbol{v}_1 \quad \dots \quad c_n k \boldsymbol{v}_n], \tag{5}$$

where $\boldsymbol{v}_i \in \mathbb{R}^3$ and $\boldsymbol{d}_i \in \mathbb{R}^3$ are respectively the thrust direction and CoM position of the $i-$th propeller in $\mathcal{F}_R$. $c_i = -1 (c_i = 1)$ if the $i-$th propeller angular velocity vector has the same direction of $\boldsymbol{v}_i (-\boldsymbol{v}_i)$ when $u_i > 0$, i.e., the propeller spins CCW (CW), and $k \in \mathbb{R}$ is the drag to lift ratio of each propeller, where we assumed all propellers to be identical.

III. Optimum OmniPlus

From the previous section, we can define a fixed propeller aerial vehicle design as the tuple $\mathcal{T} = (n, m_R, \boldsymbol{v}, \boldsymbol{d}, \boldsymbol{c}, k, u_{min}, u_{max})$ representing the number of propellers n, the platform mass m_R, the thrust direction and position of each propeller in $\mathcal{F}_R$ – $\boldsymbol{v}$ and $\boldsymbol{d}$, respectively –, the rotation direction of the corresponding propellers $\boldsymbol{c}$, the aerodynamic drag to lift coefficient k, and minimum and maximum thrust of each propeller, u_{min} and u_{max}, where $0 < u_{min} < u_{max}$.

While u_{min} and u_{max} are not shown in the previous formalism, they are crucial for any platform design to guarantee the feasibility of a desired wrench $\boldsymbol{w}_d \in \mathbb{W}$, where $\mathbb{W}$ is the set of required wrenches. As such, we can write the following condition:

$$\forall\, \boldsymbol{w}_d \in \mathbb{W} \quad \exists\, \boldsymbol{u}_d \quad s.t. \quad \boldsymbol{w}_d = \boldsymbol{F}\boldsymbol{u}_d \quad and \quad \boldsymbol{u}_d \in \mathscr{U}, \tag{6}$$

where $\mathscr{U}$ is the set of allowable control thrust, defined as the $n-$dimensional hypercube s.t. $\mathscr{U} = \bigtimes_{i=1}^{n} [u_{min}, u_{max}]$.

We denote with $\mathbf{1}$ the column vector with all ones. Its size is understood from the context. Given two vectors $\boldsymbol{x}$ and $\boldsymbol{y}$, the notations $\boldsymbol{x} \geq \boldsymbol{y}$, $\boldsymbol{x} > \boldsymbol{y}$ have to be intended componentwise.

Definition 1. *a design tuple $\mathcal{T}$ is said to be OmniPlus O_+ if one of the following equivalent conditions holds [14]*

$$\forall \boldsymbol{w} \in \mathbb{R}^6 \quad \exists \boldsymbol{u} \geq u_{min}\mathbf{1} \quad s.t. \quad \boldsymbol{F}\boldsymbol{u} = \boldsymbol{w} \tag{7}$$

$$\forall \boldsymbol{w} \in \mathbb{R}^6 \quad \exists \boldsymbol{u} \geq \boldsymbol{0} \quad s.t. \quad \boldsymbol{F}\boldsymbol{u} = \boldsymbol{w} \tag{8}$$

$$rank(\boldsymbol{F}) = 6, \quad \exists \boldsymbol{b} = [b_1 \dots b_n]^\top > \boldsymbol{0} \quad s.t. \quad \boldsymbol{F}\,\boldsymbol{b} = \boldsymbol{0} \tag{9}$$

[1] $SO(3) = \{\boldsymbol{R} \in \mathbb{R}^{3\times3} \mid \boldsymbol{R}^\top \boldsymbol{R} = \boldsymbol{I}_3, \det(\boldsymbol{R}) = 1\}$, where $\boldsymbol{I}_i \in \mathbb{R}^{i\times i}$ is the identity matrix of dimension i.

A. Allocation Strategy

Given an O_+ design, and following *condition* (9), then for any desired wrench, one may calculate a thrust $\boldsymbol{u}^*$ *s.t.* $\boldsymbol{u}^* = \boldsymbol{F}^\dagger \boldsymbol{w}_d$ where $\boldsymbol{F}^\dagger$ is the *Moore-Penrose* pseudo inverse of $\boldsymbol{F}$. As was proven in [14], $\boldsymbol{u}^*$ always has at least a negative entry, and as such violates *condition* (7).

Let us consider an ellipsoid that represents the attainable wrench space $S_w = \{\boldsymbol{w} \in \mathbb{R}^6 | \boldsymbol{w}^\top \ \Sigma \boldsymbol{w} \leq \mathbf{1}\} \subset \mathbb{R}^6$, where $\Sigma \in \mathbb{R}^{6\times 6}$ is a positive definite matrix. The set U_w maps S_w through the linear transformation $\boldsymbol{F}$ such that $U_w = \{\boldsymbol{u} \in \mathbb{R}^n | \boldsymbol{w} = \boldsymbol{F}\boldsymbol{u}, \forall \boldsymbol{w} \in S_w\}$. U_w maps S_w one to one, however, as stated in the previous paragraph, not all solutions $\boldsymbol{u}^* \in U_w$ have all positive entries, and as such $U_w \not\subset \mathscr{U}$.

Let's define a vector $\boldsymbol{b} \in null(\boldsymbol{F}) \cap \mathbb{R}^n_+$, then $\boldsymbol{b} \perp \boldsymbol{u}^*$. Any solution such that $\boldsymbol{u}^{**} = \boldsymbol{u}^* + \lambda \boldsymbol{b}$ with $\lambda > 0 \in \mathbb{R}$ satisfies $\boldsymbol{w}_d = \boldsymbol{F}\boldsymbol{u}^{**}$. As such, the objective of the allocation strategy would be to find λ such that $\boldsymbol{u}^{**} \in \mathscr{U}$ as follows:

$$\lambda \ = \ \underset{\boldsymbol{u}^{**}\in\mathscr{U}}{\operatorname{argmin}} \ \|\boldsymbol{u}^{**}(\boldsymbol{u}^*, \boldsymbol{b})\| \ = \ \underset{\boldsymbol{u}^{**}\in\mathscr{U}}{\operatorname{argmin}} \ \|\boldsymbol{u}^* + \lambda \boldsymbol{b}\|. \tag{10}$$

The control thrust found in (10) satisfies $\boldsymbol{u}^{**} \in U^*_w$, where $U^*_w = U_w \cap \mathscr{U}$. It is noted that U^*_w also maps S_w one to one, and as such, in what follows we refer to $\boldsymbol{u}^{**}(\boldsymbol{w})$ as the control thrust in U^*_w that allows the platform to apply wrench $\boldsymbol{w}$.

Definition 2. *an O_+ design is said to be optimal if its space U^*_w has minimum eccentricity, and if its propellers equally share the effort to keep $\boldsymbol{u}^{**} \in \mathscr{U}$ calculated in* (10).

Minimizing the eccentricity of U^*_w allows the platform to apply lower maximum thrust for each desired wrench since the platform will be sharing the load equally among its propellers; this problem can be solved by minimizing the condition number of $\Sigma^{-1}\boldsymbol{F}$. On the other hand, to satisfy the second condition of *Definition* 2, it is easy to be convinced that the best choice is $\boldsymbol{b} = \mathbf{1}$. For more details we refer the reader to [14].

IV. Parameter Optimization

In this section we detail the choice of parameters that allow the design $\mathscr{T}$ to satisfy the conditions and requirements mentioned above. First, we make the following assumptions:

- platform dimensions are chosen separately and fixed throughout the optimization,
- all motors and propellers used in the platform are identical,
- motor and propeller choice is made separately from this optimization problem,
- propeller rotation directions are chosen prior to the optimization, with these directions alternating between one propeller and the next, *i.e.* $c_i = (-1)^i$ for $i = 1 \dots n$.

With these assumptions, we can clearly see that the *etero-vectoring* part of $\mathscr{T}$ (n, m_R, $\boldsymbol{d}$, $\boldsymbol{c}$, k, u_{min}, u_{max}) is fixed, in addition to the norm of the vectoring part $\|\boldsymbol{v}_i\|$ for $i = 1 \dots n$, while the optimization problem should choose the direction of the vectoring part ($\boldsymbol{v}$). It is noted that $\|\boldsymbol{v}_i\| = 1$ as the allocation matrix $\boldsymbol{F}$ is assumed to map wrench $\boldsymbol{w}$ to propeller thrust $\boldsymbol{u}$.

To highlight the optimization problem, let us rewrite $\boldsymbol{F}_1$ and $\boldsymbol{F}_2$ as follows:

$$\boldsymbol{F}_1 = [\boldsymbol{I}_3 \boldsymbol{v}_1 \dots \boldsymbol{I}_3 \boldsymbol{v}_n] \tag{11}$$

$$\boldsymbol{F}_2 = [(S(\boldsymbol{d}_1) + c_1 k \boldsymbol{I}_3)\boldsymbol{v}_1 \dots (S(\boldsymbol{d}_n) + c_n k \boldsymbol{I}_3)\boldsymbol{v}_n] \tag{12}$$

then we can rewrite the second part of (9) as:

$$\underbrace{\begin{bmatrix} \boldsymbol{I}_3 b_1 & \dots & \boldsymbol{I}_3 b_n \\ (S(\boldsymbol{d}_1) + c_1 k \boldsymbol{I}_3) b_1 & \dots & (S(\boldsymbol{d}_n) + c_n k \boldsymbol{I}_3) b_n \end{bmatrix}}_{\boldsymbol{A}(n, \boldsymbol{d}, \boldsymbol{c}, k, \boldsymbol{b})} \boldsymbol{v} = \mathbf{0}, \tag{13}$$

where $\boldsymbol{I}_i$ is the i-by-i *identity matrix* .

Following this formalism, the O_+ parameter optimization can be written as follows:

$$\min \ cond(\Sigma^{-1}\boldsymbol{F}) \tag{14}$$

subject to the following constraints

$$\boldsymbol{v}^\top \boldsymbol{D}_1 \boldsymbol{v} = 1, \dots, \boldsymbol{v}^\top \boldsymbol{D}_n \boldsymbol{v} = 1 \tag{15}$$

$$rank(\boldsymbol{F}(\boldsymbol{c}, k, \boldsymbol{d}, \boldsymbol{v})) = 6 \tag{16}$$

$$\boldsymbol{A}(n, \boldsymbol{d}, \boldsymbol{c}, k, \mathbf{1})\boldsymbol{v} = \mathbf{0} \tag{17}$$

where $\boldsymbol{D}_i = diag(\boldsymbol{D}_{i1} \dots \boldsymbol{D}_{in})$ is a $3n$-by-$3n$ diagonal matrix, with $\boldsymbol{D}_{ij} = 0$ if $j \neq i$ and $\boldsymbol{D}_{ii} = \boldsymbol{I}_3$ otherwise.

We note that in the choice of the propeller placements, we chose all propellers to be coplanar, placed in a star shape with the first propeller arm along $\boldsymbol{x}_R$, *i.e.* $\boldsymbol{d}_1 = [d, 0, 0]^\top$, and $\boldsymbol{d}_i = \boldsymbol{d}_1 \boldsymbol{R}_{\boldsymbol{z}}(2\pi(i-1)/n)$ for $i = 2 \dots n$, where d is the norm of the arm connecting O_R to the CoM of any propeller, and $\boldsymbol{R}_{\boldsymbol{z}}$ is the transformation matrix corresponding to the rotation about $\boldsymbol{z}_R$.

As the aim of this paper is to build an omnidirectional platform, it is desired that the force and moment ellipsoids to resemble a sphere, where the platform will be invariant to its flight direction. As such we choose Σ of the form

$$\Sigma = \begin{bmatrix} \sigma_{\boldsymbol{f}} \boldsymbol{I}_3 & \mathbf{0}_{3\times 3} \\ \mathbf{0}_{3\times 3} & \sigma_{\boldsymbol{m}} \boldsymbol{I}_3 \end{bmatrix} \tag{18}$$

where $\sigma_{\boldsymbol{f}}, \sigma_{\boldsymbol{m}} \in \mathbb{R}_{>0}$.

Finally, we analyze the maximum propeller thrust u^d_{max} while the platform is in hover, where we define

Definition 3. *hovering (or* static hovering*) as the ability of the platform to stabilize its position and orientation for some orientation $\boldsymbol{R}_d \in SO(3)$ with zero linear and angular velocity, i.e. ($\boldsymbol{p}^d_R$, $\boldsymbol{R}_d$, $\boldsymbol{v}^d_R$, $\boldsymbol{\omega}^d_R$) = ($\boldsymbol{p}^d_R$, $\boldsymbol{R}_d$, $\mathbf{0}$, $\mathbf{0}$).*

Hovering is of particular interest for the design as it is a base point for the platform to apply forces and moments in any direction. The analysis of u^d_{max} is required for the choice of motor and it is an important feature to study the feasibility of the design.

The chosen Σ, and the ensuing minimization of $cond(\Sigma^{-1}\boldsymbol{F})$, enforces a uniformity in the platform's generated force (moment) about its corresponding directions,

and as such guarantees invariance of the platform to $\boldsymbol{R}$ at hovering.

While hovering, the thrust of each propeller can be calculated as

$$\boldsymbol{u}_d(\boldsymbol{R}_d) = \boldsymbol{u}_d^{**}\left(\begin{bmatrix} m_R\, g\, \boldsymbol{R}_d\, \boldsymbol{e}_3 \\ \boldsymbol{0}_3 \end{bmatrix}\right) \tag{19}$$

Due to the invariance of the platform to its hovering direction and to the chosen optimization constraints, it is straight forward to prove that

$$u^d_{max} = \max\ \boldsymbol{u}_d(\boldsymbol{R}_d) = \max\ \boldsymbol{u}_d(\boldsymbol{I}) \tag{20}$$

While in theory maximum propeller thrust should be the same irrespective of the hovering orientation, in practice the condition number never reaches unity, and as such there is always a difference between the max $\boldsymbol{u}_d(\boldsymbol{R}_d)$ at different $\boldsymbol{R}_d$, and as such, u^d_{max} is found with a grid search algorithm over possible orientations.

V. Controller

Given a desired position and orientation $\boldsymbol{p}^d_R(t)$ and $\boldsymbol{R}_d(t)$, the control strategy is straight forward as the allocation matrix $\boldsymbol{F}$ is full rank, and as such the platform is fully actuated. The desired wrench is calculated as the one that brings the platform to the desired position and orientation (along with their corresponding derivates) while compensating for gravity and gyroscopic moments. As such the desired wrench can be written as follows:

$$\boldsymbol{w}^d = \boldsymbol{G}^{-1}\begin{bmatrix} m_R(g\boldsymbol{e}_3 + \dot{\boldsymbol{v}}^d_R) + \boldsymbol{K}_P\boldsymbol{e}_p + \boldsymbol{K}_D\dot{\boldsymbol{e}}_p + \boldsymbol{K}_{IP}\int_0^t \boldsymbol{e}_p \\ \boldsymbol{\omega}_R \times \boldsymbol{J}_R\boldsymbol{\omega}_R + \boldsymbol{K}_{\boldsymbol{R}}\boldsymbol{e}_{\boldsymbol{R}} + \boldsymbol{K}_\omega\boldsymbol{e}_\omega + \boldsymbol{K}_{I\boldsymbol{R}}\int_0^t \boldsymbol{e}_{\boldsymbol{R}} \end{bmatrix} \tag{21}$$

where $\boldsymbol{K}_P, \boldsymbol{K}_D, \boldsymbol{K}_{IP}, \boldsymbol{K}_{\boldsymbol{R}}, \boldsymbol{K}_\omega$ and $\boldsymbol{K}_{I\boldsymbol{R}}$ are diagonal positive definite matrices $\in \mathbb{R}^{3\times3}$ representing the controller tunable gains. $\boldsymbol{e}_p = \boldsymbol{p}^d_R - \boldsymbol{p}_R$, $\boldsymbol{e}_\omega = \boldsymbol{\omega}^d_R - \boldsymbol{\omega}_R$ and $\boldsymbol{e}_{\boldsymbol{R}} = 1/2(\boldsymbol{R}_d^\top\boldsymbol{R} - \boldsymbol{R}^\top\boldsymbol{R}_d)^\wedge$, where $[.]^\wedge$ is the inverse skew symmetric operator. Then for each desired wrench, a control thrust is calculated as described earlier in (10).

A. State Estimation

The platform is endowed with and IMU that captures the platforms specific linear acceleration and angular velocity. Furthermore, its position and orientation are tracked with a motion capture system.

All measurements from the IMU are filtered with the regression-based filter introduced in [15]. The filter is designed to reduce the noise caused by the propellers vibration; however, as the motors are controlled in open-loop (*i.e.* propeller rotational velocities are not measured), the filter fit the second order polynomial to the IMU signal without separation between its signal and noise constituents.

Both filtered IMU measurements and motion capture measurements are fused using an Unscented Kalman Filter (UKF) [16] to retrieve the full pose estimate of the platform.

Component	weight per unit [g]	# units	weight [g]
Motors	40	7	280
Propellers	5	7	35
Electronics	200	–	200
Mechanical parts	350	–	350
Battery	214	–	214
Total			1079

TABLE I: Representing the estimated weight of each of the platform components prior to its final design and construction. It should be noted that the weight of parts that are certainly used were reported as they are, while others are estimated.

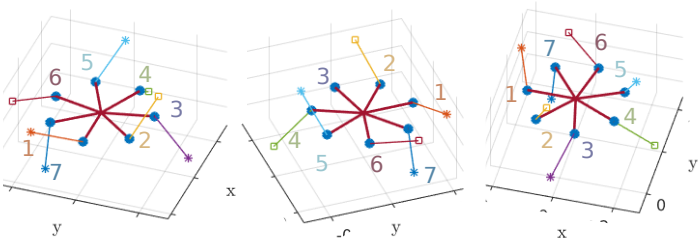

Fig. 2: Optimized propeller direction of the O^7_+ design, with $n = 7$, $d = 0.16\,[m]$ and $k = 0.002\,[m]$ at $cond(\Sigma^{-1}\boldsymbol{F}) = 2.052$.

VI. Prototype

For our prototype we chose to construct a platform with $n = 7$, the least number of uni-directional propellers necessary to achieve omnidirectional thrust. The platform is built to be the smallest possible to increase the platforms stability by reducing any possible oscillations in the arms connecting the motors to the body; as such, we chose an arm length $d = 0.16$ [m]. We then chose 5" propellers, as it is the largest diameter that can be installed on the platform without any collision between adjacent propellers. The propellers we chose enforced a drag to lift coefficient $k = 0.002$ [m], and a lift coefficient $k_f = 0.5e-4$[N/Hz^2]. Finally, the wrench ellipsoid was chosen such that $\Sigma = diag([1,1,1,0.5,0.5,0.5])$. We estimated the platform mass before the platform construction to be around 1.1 [kg] following the component-wise weight estimation shown in table I.

A. Numerical Optimization

The O_+ optimization algorithm calculated the vectoring part of the design, and reached a minimum condition number of $cond(\Sigma^{-1}\boldsymbol{F}) = 2.052$, with a vectoring vector as follows:

$$\boldsymbol{v} = \begin{bmatrix} 0.36 & -0.35 & 0.29 & -0.81 & -0.37 & 0.78 & 0.10 \\ -0.90 & 0.44 & 0.76 & -0.12 & 0.45 & -0.57 & -0.07 \\ 0.25 & 0.83 & -0.58 & -0.58 & 0.81 & 0.26 & -0.99 \end{bmatrix}, \tag{22}$$

The above thrust directions are illustrated in Fig. 2.

With the current parameters, $u^d_{max} = 11.18\,[N]$, corresponding to a maximum rotational speed of $W_{max} = 472$ [Hz] for the chosen propellers; as such we chose a motor that can

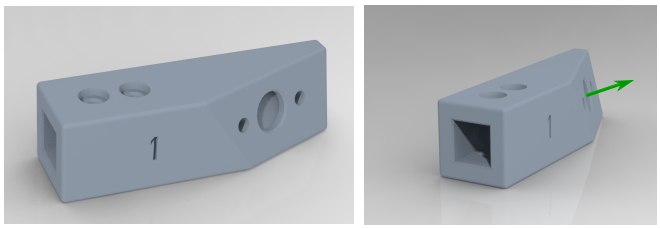

Fig. 3: CAD design of the motor adapter for motor # 1. The adapter is designed to fasten the motor to the body frame at position $\boldsymbol{d}_1$ and orientation $\boldsymbol{v}_1$ in $\mathcal{F}_R$.

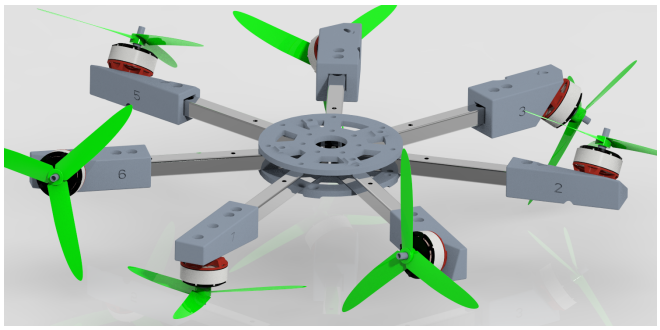

Fig. 4: CAD design showing the platform body assembly. The body assembly shows the motors and propellers connected to the body frame with aluminum bars, where each motor was fastened to the corresponding bar with a CAD designed adapter similar to the one shown in fig. 3. Each of the shown adapters was designed to fit the corresponding orientation $\boldsymbol{v}_i$ in $\mathcal{F}_R$.

provide a peak thrust of 14N with the chosen propellers, at which the motor is required to rotate at 530 [Hz].

The chosen motor is controlled in PWM via an Electronic Speed Controller (ESC), *i.e.* , the motor is controlled in open-loop, where the thrust generated at each PWM was identified with a force torque sensor. Finally, the PWMs delivered to the ESCs are generated using an onboard microcontroller.

B. Platform Implementation

The platform body is constructed with 7 aluminum bars connecting the CoM of the platform to the CoM of the propellers. Each propeller is connected with a separate arm to ensure the stability of the platform. Aluminum bars are fastened together using 3*D* printed plates connected to one of their edges, while the second edge is connected to a 3*D* printed adapter that ensures the motors' connection at the calculated direction. Fig. 3 shows the CAD drawing of one of the adapters, while Fig. 4 shows the CAD drawing of the body frame assembly.

Finally, the necessary electronics and motion capture markers are placed on top of the platform, with the full prototype shown in Fig. 1.

The final weight of this setup without a battery is measured at $m_R = 0.835$ [kg].

C. Design Drawbacks

The platform prototype as presented above exhibits the following drawbacks that can affect its performance:

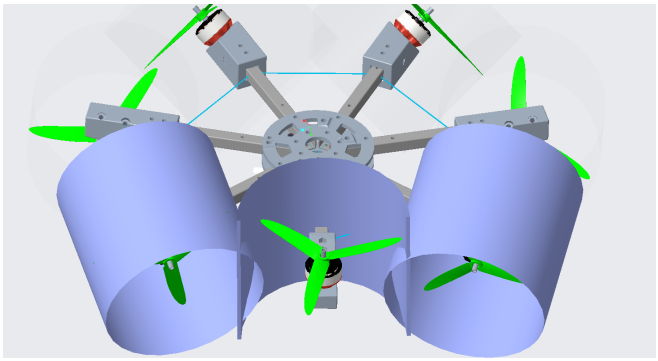

Fig. 5: Example intersection between adjacent propeller airflow cylinders, showing the intersection between 7th propeller airflow cylinder with the airflow cylinders of the 1st and 6th propeller.

- Propeller open-loop control: as the propellers are controlled in open-loop, the propeller speed is not guaranteed, and correspondingly the individual motor thrust, and the collectively applied wrench can differ from the desired one.
- Propeller airflow cylinder intersection, where we define the airflow cylinder as the cylinder containing the corresponding propeller, of radius equal to the propellers', and direction similar to the corresponding propeller. As the propellers are placed close to each other, with each producing thrust in *any* direction, it is impossible for the airflow cylinders of adjacent propellers not to intersect as shown in Fig. 5. This intersection affects their aerodynamics, as propellers have to withdraw air from the inflow/outflow of their adjacent propellers instead of withdrawing air from the free stream assumed static. It should be noted that it is difficult to estimate the effect of this intersection, as the change in the thrust produced by each propeller will depend on the amount of thrust provided by the adjacent propeller.

While these drawbacks can induce an error in the applied wrench, we assume it equivalent to an external disturbance that can be compensated by the feedback controller shown in section V.

VII. Dynamic Simulation

To assess the performance and flyability of the prototype described in section VI, we simulated its dynamical system in Matlab/Simulink with the estimated mass. The simulation is made closer to reality with the addition of measurement noise and signal delays.

Figure 6 shows the performance of the platform's flight with $\boldsymbol{z}_R$ circling the unit radius sphere. This figure shows that the platform is able to fly while in a variety of orientations. The simulation also shows that the platform can apply independent force and moments, and as such, orient $\mathcal{F}_R$ independently of its translation, while the propeller rotational velocities are kept within the allowable range.

VIII. Wrench Tests

To assess the discrepancy between the nominal model and the built prototype, a force-torque sensor was used to

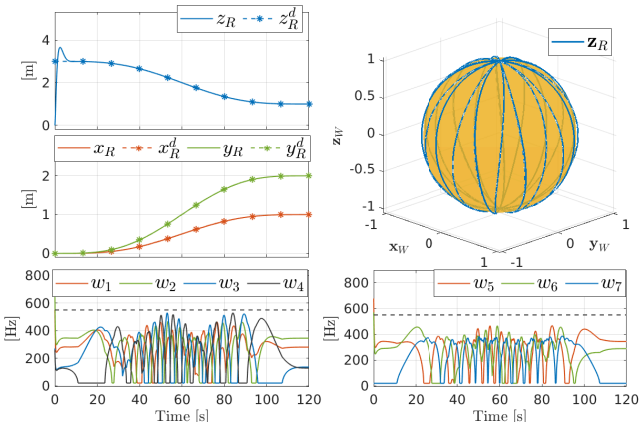

Fig. 6: Tracking results of the simulated platform while following a desired position and orientation. The platform orientation is chosen such that $\boldsymbol{z}_R$ circles the unit sphere multiple times, while the position is chosen to change smoothly and simultaneously on all axes. A step change in the z-position is required at time $t = 0s$, where the platform is required to lift from the height of 0 [m] to 4 [m]. The figure also shows the propeller rotational velocities w_i for $i = 1 \ldots 7$, where the dashed line constitutes the limiting maximum velocity.

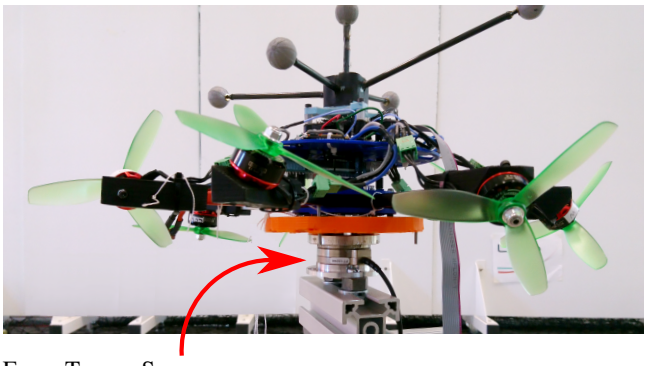

Fig. 7: Platform fixed to the force torque sensor.

test	$\boldsymbol{f}_d$	$\boldsymbol{f}error$	$\boldsymbol{m}_d$	$\boldsymbol{m}error$
1	$[0\,0\,8]$	$[0.4\,+0.0\,-0.2]$	$[0\,0\,0]$	$[-0.1\,+0.1\,+0.1]$
2	$[4\,2\,8]$	$[0.0\,-0.1\,-0.3]$	$[0\,0\,0]$	$[-0.1\,+0.3\,-0.2]$
3	$[0\,4\,8]$	$[0.2\,-0.3\,-1.1]$	$[0\,0\,0]$	$[-0.3\,+0.1\,+0.0]$
4	$[0\,0\,8]$	$[0.6\,-0.1\,-0.6]$	$[0.2\,0\,0]$	$[-0.1\,+0.1\,+0.1]$
5	$[0\,0\,8]$	$[0.3\,-0.3\,-0.4]$	$[0\,0.2\,0]$	$[-0.0\,-0.1\,+0.1]$
6	$[0\,0\,8]$	$[0.3\,-0.1\,-0.4]$	$[0\,0\,0.2]$	$[-0.0\,+0.1\,-0.0]$

TABLE II: Representing the nominally applied force $\boldsymbol{f}_d$ and moment $\boldsymbol{m}_d$, and their respective measured error.

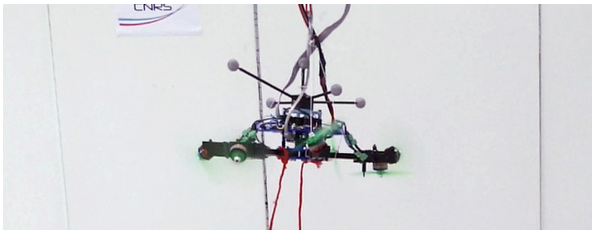

(a) Horizontal hovering

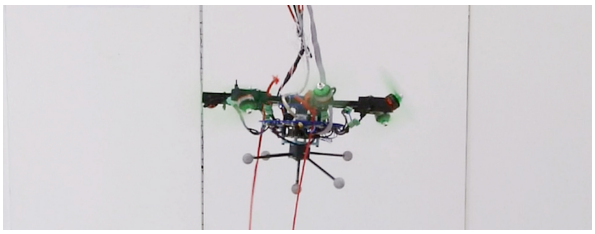

(b) Upside down hovering

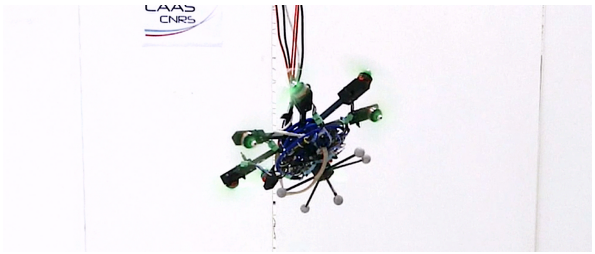

(c) Tilted hovering $\phi_d = 130°$

Fig. 8: Preliminary hovering tests of the prototype platform: a) platform hovering horizontally, b) platform hovering upside down, c) platform hovering at a tilted orientations such that $\phi_d = 130°$.

measure the generate wrench in a static experiment as shown in Fig. 7. Table II shows the force and moment constituents of the desired nominal wrench $\boldsymbol{w}_d$ and the corresponding error between the measured and nominal wrench $\boldsymbol{w}_{error} = w_{measured} - w_d$.

We can observe from the data in table II an error between the measured and nominal values of the applied wrench; it can also be observed that the value of this error changes depending on the desired nominal wrench. While we could not identify clearly the cause of these errors, they were actually expected due to the motor speed control and aerodynamic interaction between adjacent propellers, in addition to manufacturing imperfections (see section VI-C).

IX. Experiments

A. System Setup

As stated in section V-A, the platform is endowed with an IMU, which exports the raw specific linear acceleration and angular velocity measurements at 1 [kHz]; in addition, the platform position and orientation are tracked with a motion capture system at 100 [Hz]. Both measurements are fused by a UKF running at 1 [kHz], and providing an estimate of the platform state. The platform controller is implemented in Matlab/Simulink at 500 [Hz], while the onboard microcontroller delivers the desired PWM to the ESCs. Most software (excluding the controller), including those used for the communication between Matlab and the platform, are developed in C++ using Genom3 [17], a code generator and formal software component description language that allows assembling middleware-independent components in a modular system. These software can be found here: `https://git.openrobots.org/projects/telekyb3`

The platform is top-connected to a power supply cable, in

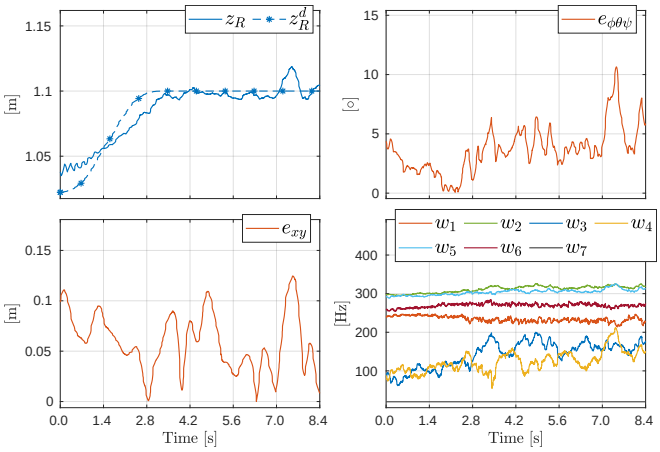

Fig. 9: Performance of the platform while hovering horizontally: (top-left) shows the desired and estimated platform height, (top-right) shows the average angular error, (bottom-left) shows the average *xy* error, and (bottom-right) shows the propeller rotational velocities.

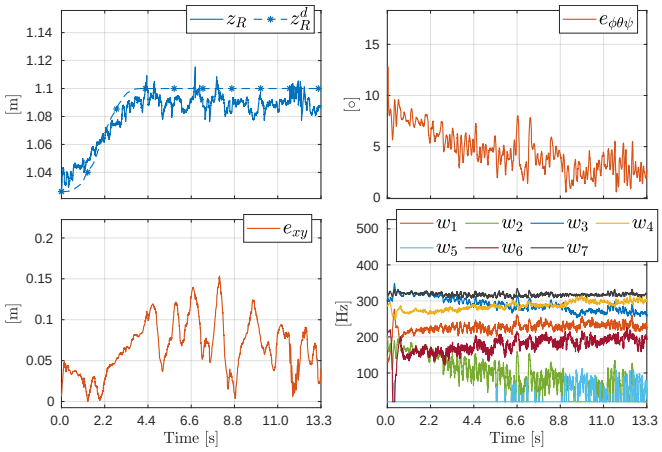

Fig. 10: Performance of the platform while hovering with z_R pointing in the negative z_W direction, *i.e.* , $\phi_d = 180°$: (top-left) shows the desired and estimated platform height, (top-right) shows the average angular error, (bottom-left) shows the average *xy* error, and (bottom-right) shows the propeller rotational velocities.

addition to multiple data cables allowing the back and forth communication with the off-board controller PC.

B. Hovering

To preliminarily test the omnidirectional flight ability of the platform, we ask the vehicle to lift off from its hanged position and hover in place in multiple orientations as shown in Fig. 8a through 8c. The performance of the platform in each of the desired orientations is shown in Figures 9 through 11. These figures show that the platform is able to hover horizontally, upside down, and at a tilted angle. Furthermore, for these orientations, the desired propeller rotational velocities are within the acceptable range.

Remark 1. In all these experiments, the propeller rotational velocities are within the acceptable range. Moreover, the maximum propeller rotational velocity is around 380 [Hz], far from the maximum allowed rotational velocity of 550 [Hz].

Remark 2. While the platform is able to hover at these orientations, there is a noticeable tracking error in all experiments even if the controller gains have been tuned specifically for each experiment to reduce tracking error while assuring the platform stability.

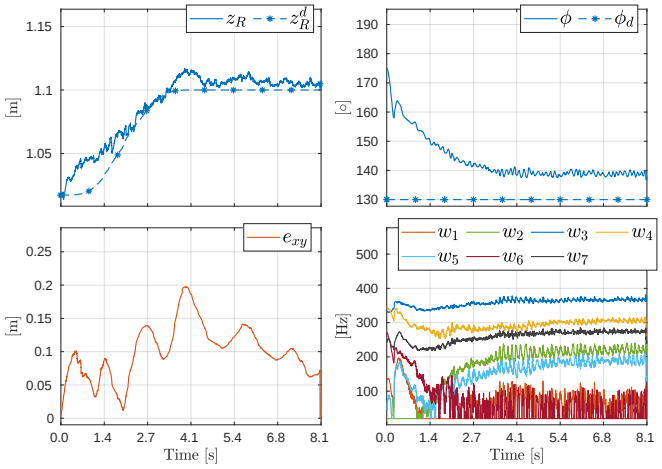

Fig. 11: Performance of the platform while hovering at a tilted orientation such that $\phi_d = 130°$, $\theta_d = 0°$ $\psi_d = 90°$: (top-left) shows the desired and estimated platform height, (top-right) shows the desired and estimated platform roll, (bottom-left) shows the average *xy* error, and (bottom-right) shows the propeller rotational velocities. The platform starts its maneuver while being oriented near upside down, *i.e.* $\phi(t = 0s) \approx 180°$.

X. CONCLUSIONS

In this paper we have presented a novel prototype of O_+ UAV with 7 propellers. To the knowledge of the authors, the design is the first of its kind. We conducted an experimental campaign to assess the model and the prototype. Our experiments show that the platform is able to hover in many directions. We have realized from our tests that there is a discrepancy between the nominal desired wrench and the one actually applied by the platform due to multiple drawbacks in the design such as : 1) open-loop control of the propeller rotational velocities, 2) and aerodynamic interactions between adjacent propellers due to the small size of the frame. While the aerodynamic interactions are caused by the closeness of the propellers, the open-loop control of the propellers is necessary to ensure such high speed rotational velocity of the propellers, where beyond a certain propeller rotational velocity the currently available ESCs can no longer close the corresponding control loop for computational limits.

In the future, we aim at ameliorating the design along the following lines

- Reduce the weight of the platform by replacing aluminum bars with lighter carbon fiber material. This will allow the platform to fly with lower propeller rotational velocities, and as such be able to achieve close-loop control of the propellers.
- Increase the arm length distance in the platform to

reduce the aerodynamic interactions between propellers.

- Implement an adaptive/learning based controller that can compensate for the unmodeled aerodynamic interactions.

REFERENCES

[1] A. Ollero, G. Heredia, A. Franchi, G. Antonelli, K. Kondak, A. Sanfeliu, A. Viguria, J. R. Martinez-de Dios, F. Pierri, J. Cortés, A. Santamaria-Navarro, M. A. Trujillo, R. Balachandran, J. Andrade-Cetto, and A. Rodriguez, "The AEROARMS project: Aerial robots with advanced manipulation capabilities for inspection and maintenance," *IEEE Robotics & Automation Magazine, Special Issue on Floating-base (Aerial and Underwater) Manipulation*, vol. 25, no. 4, pp. 12–23, 2018.

[2] A. Ollero, "Aerial robotics cooperative assembly system (arcas): First results," in *Aerial Physically Acting Robots (AIRPHARO) Workshop, IROS*, 2012, pp. 7–12.

[3] R. Mahony, V. Kumar, and P. Corke, "Multirotor Aerial Vehicles: Modeling, Estimation, and Control of Quadrotor," *IEEE Robotics & Automation Magazine*, vol. 19, no. 3, pp. 20–32, 2012.

[4] M. Faessler, A. Franchi, and D. Scaramuzza, "Differential flatness of quadrotor dynamics subject to rotor drag for accurate tracking of high-speed trajectories," *IEEE Robotics and Automation Letters*, vol. 3, no. 2, pp. 620–626, 2018.

[5] M. Ryll, G. Muscio, F. Pierri, E. Cataldi, G. Antonelli, F. Caccavale, D. Bicego, and A. Franchi, "6D interaction control with aerial robots: The flying end-effector paradigm," *The International Journal of Robotics Research*, vol. 38, no. 9, pp. 1045–1062, 2019.

[6] H. Romero, S. Salazar, A. Sanchez, and R. Lozano, "A new UAV configuration having eight rotors: dynamical model and real-time control," in *46th IEEE Conf. on Decision and Control*, New Orleans, LA, Dec. 2007, pp. 6418–6423.

[7] M. Ryll, D. Bicego, and A. Franchi, "Modeling and control of FAST-Hex: a fully-actuated by synchronized-tilting hexarotor," in *2016 IEEE/RSJ Int. Conf. on Intelligent Robots and Systems*, Daejeon, South Korea, Oct. 2016, pp. 1689–1694.

[8] M. Ryll, H. H. Bülthoff, and P. Robuffo Giordano, "A novel overactuated quadrotor unmanned aerial vehicle: modeling, control, and experimental validation," *IEEE Trans. on Control Systems Technology*, vol. 23, no. 2, pp. 540–556, 2015.

[9] Y. Long and D. J. Cappelleri, *Omnicopter: A Novel Overactuated Micro Aerial Vehicle*. Heidelberg: Springer International Publishing, 2013, pp. 215–226.

[10] D. Brescianini and R. D'Andrea, "Design, modeling and control of an omni-directional aerial vehicle," in *2016 IEEE Int. Conf. on Robotics and Automation*, Stockholm, Sweden, May 2016, pp. 3261–3266.

[11] S. Park, J. J. Her, J. Kim, and D. Lee, "Design, modeling and control of omni-directional aerial robot," in *2016 IEEE/RSJ Int. Conf. on Intelligent Robots and Systems*, Daejeon, South Korea, 2016, pp. 1570–1575.

[12] E. Dyer, S. Sirouspour, and M. Jafarinasab, "Energy optimal control allocation in a redundantly actuated omnidirectional uav," in *2019 IEEE Int. Conf. on Robotics and Automation*, Montreal, Canada, may 2019.

[13] M. Hamandi, F. Usai, Q. Sablé, N. Staub, M. Tognon, and A. Franchi, "Survey on Aerial Multirotor Design: a Taxonomy Based on Input Allocation," Jan. 2020, working paper or preprint. [Online]. Available: https://hal.archives-ouvertes.fr/hal-02433405

[14] M. Tognon and A. Franchi, "Omnidirectional aerial vehicles with unidirectional thrusters: Theory, optimal design, and control," *IEEE Robotics and Automation Letters*, vol. 3, no. 3, pp. 2277–2282, 2018.

[15] M. Hamandi, M. Tognon, and A. Franchi, "Direct acceleration feedback control of quadrotor aerial vehicles," *2020 IEEE Int. Conf. on Robotics and Automation*.

[16] E. A. Wan and R. Van Der Merwe, "The unscented kalman filter for nonlinear estimation," in *Proceedings of the IEEE 2000 Adaptive Systems for Signal Processing, Communications, and Control Symposium (Cat. No. 00EX373)*. Ieee, 2000, pp. 153–158.

[17] A. Mallet, C. Pasteur, M. Herrb, S. Lemaignan, and F. Ingrand, "Genom3: Building middleware-independent robotic components," *2010 IEEE International Conference on Robotics and Automation*, pp. 4627–4632, 2010.